Available online at www.sciencedirect.com

ScienceDirect

journal homepage: www.elsevier.com/locate/he

Cavern integrity for underground hydrogen storage in the Brazilian pre-salt fields

Williams Dias [a,b], *Deane Roehl* [a,b,*], *Cristian Mejia* [b], *Paul Sotomayor* [b]

[a] *Department of Civil and Environmental Engineering, Pontifical Catholic University of Rio de Janeiro, 225 Marquês de São Vicente Street, Gávea, 22451-900, Rio de Janeiro, RJ, Brazil*

[b] *Tecgraf Institute/PUC-Rio, 225 Marquês de São Vicente Street, Gávea, 22451-900, Rio de Janeiro, RJ, Brazil*

HIGHLIGHTS

- Simulation of underground hydrogen storage considering thermomechanical effects.
- Coupling thermomechanical finite element analysis with thermodynamics gas simulator.
- Assessment of salt rock integrity considering dilatancy and permeability evolution.
- Cavern integrity analysis using a unified analytical solution for P and T° variations.
- Simulating different scenarios of underground hydrogen storage in Brazilian pre-salt caverns.

GRAPHICAL ABSTRACT

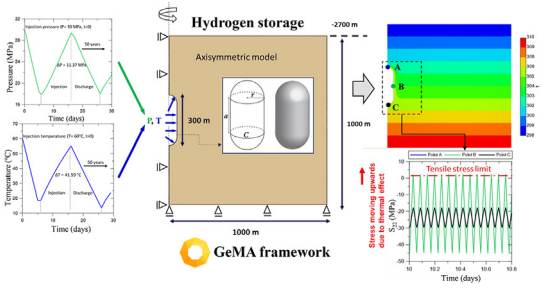

ARTICLE INFO

Article history:
Received 17 December 2022
Received in revised form
23 February 2023
Accepted 19 March 2023
Available online xxx

Keywords:
Hydrogen storage
Creep
Salt cavern
Thermo-mechanical analysis

ABSTRACT

Over the years, energy has depended on petroleum-based fuels. However, global warming and the energy crisis have drastically impacted the markets. It urges investing in renewable energy resources, such as hydrogen. Therefore, this work focuses on the hydrogen storage process in salt caverns, as these rocks have relevant properties, such as low permeability, relevant creep, and self-healing. A workflow for cavity integrity analysis is proposed. Hydrogen storage provokes variations in temperature and pressure inside the cavern. The gas thermodynamics is represented through a diabatic solution, which updates the gas pressure and temperature at each time step. The thermomechanical formulation is implemented into an in-house framework GeMA, which couples different physics. Four case studies are analyzed, and the discussions compared mechanical and thermomechanical models. Results demonstrate the importance of thermal effects, as

* *Corresponding author*. Department of Civil and Environmental Engineering, Pontifical Catholic University of Rio de Janeiro, 225 Marquês de São Vicente Street, Gávea, 22451-900, Rio de Janeiro, RJ, Brazil.

E-mail addresses: willdias@tecgraf.puc-rio.br (W. Dias), deane@tecgraf.puc-rio.br (D. Roehl), crisms@tecgraf.puc-rio.br (C. Mejia), paulortega@tecgraf.puc-rio.br (P. Sotomayor).

https://doi.org/10.1016/j.ijhydene.2023.03.292

temperature amplitudes may compromise rock integrity, for instance, inducing tensile stresses and affecting permeability.

Introduction

The current energy sources are highly dependent on petroleum-based fuels and electricity powered by fossil fuels, which are not sustainable and contribute to global warming (greenhouse effect). Additionally, the recent energy crisis, which emerged from the war between Ukraine and Russia, has shown the importance of having alternative energies to assure supply and market equilibrium. Hydrogen can be a suitable option to reduce the dependency on fossil fuels and accelerate the energy mix transition to low-carbon energy sources [1,2]. Besides, hydrogen can be produced from different processes, for example, thermochemical, electrolytic, biological, or direct solar water splitting. Regarding its storage, underground hydrogen storage (UHS) has risen as a good alternative because of its high capacity to accommodate a significant gas volume, cost effectivity, and safety [3,4]. Several hydrogen storage projects have been conducted worldwide in the last decade - Roads2HyCOM (2005), Hychico (2006), H2STORE (2012), ANGUSþ (2013), InSpEE (2015), and HyINTEGER (2016) [3].

Among the UHS options, the most common are depleted gas reservoirs, aquifers, or artificial salt caverns. However, depleted gas reservoirs and aquifers have disadvantages regarding pure hydrogen storage, cushion gas requirements, engineering conditions, and costs [5]. In this context, salt caverns are an ideal medium to store gas due to the intrinsic characteristics of salt rocks, such as low porosity and permeability, high water solubility (ideal to build and shape caverns), relevant creep and self-healing properties [6–8]. Laboratory experiments show permeabilities below 10^{-20} m^2, and field measurements give values below 10^{-18} m^2, even in the presence of inhomogeneities and local disturbances [9–11]. The successful experience of more than 80 years with liquid/gaseous hydrocarbons [12] and 50 years with hydrogen [3] indicates salt cavern as a viable and safe storage option.

A literature review of UHS reveals the Teeside site in the United Kingdom as the first UHS deposit in the world. It has been operating since the 1970s, with a total volume of 210,000 m^3 [3]. The thermodynamics of salt caverns containing brine, oil, natural gas, air, or hydrogen have also been investigated [13]. The heat capacity is much smaller in a gas cavern, temperature evolution is much faster, and heat transfer from the rock mass is relevant. Coupled thermo-mechanical analyses were performed by Ref. [14] to understand how large temperature amplitudes in the working gas may lead to tensile stresses at the cavern walls. Reducing the frequency of the storage cycles is an option to maintain safe temperature conditions. Caglayan et al. (2020) [15] analyzed the salt cavern potential for hydrogen storage across Europe. The assessment considered the land eligibility constraints derived from a review of the relevant literature, distributed the caverns across suitable locations, and finally estimated the individual cavern storage capacity by factoring in the salt formation characteristics in terms of thermodynamic storage considerations. Zivar, Kumar, and Foroozesh [3] investigated the principal aspects related to UHS projects: worldwide operating and potential sites, salt rock properties, monitoring mechanisms, optimization of injection-withdrawal strategies, microbial/geochemical activities, physics of hydrogen flow in porous media, and hydrodynamics (rock-fluid and fluid-fluid interactions). AbuAisah et al. [16] focused on hydrogen transport in rock salt during cycling using a fully coupled thermo-hydraulic framework. Results demonstrated that the amount of hydrogen lost into the surrounding rock salt was insignificant. However, it is essential to highlight that permeability changes in the host rock (for instance, due to thermal fractures) may favor gas/fluid losses [17]. The feasibility of UHS in Chinese salt caverns was carried out by Liu et al. [5]. The process included the analysis of site geological conditions, a numerical simulation model to verify the stability and applicability of the proposed caverns, and a discussion of technical/economic aspects. Lankof, Urbańczyk, and Tarkowski [2] proposed a methodology to assess salt domes for potential hydrogen storage. The work considered the size of the storage caverns, their depth, the influence of convergence, and the geological structure of the selected salt domes.

There are just a few studies in Brazil regarding gas storage in underground areas [18–21], all of which apply only to natural gas or CO_2 storage. Firme, Roehl, and Romanel [15] extensively reviewed salt caverns' history and the fundamentals of their mechanical behavior. Simulations demonstrated that the salt cavern remained tight, thereby safe under the operating conditions. All the referred studies focused only on the mechanical behavior, with the gas pressure ranging between minimum and maximum values. However, the pressure amplitudes provoke gas heating or cooling, and thermal effects may be relevant. These effects may induce tensile stresses and an increase in cavern convergence, as evidenced by Ref. [14].

Therefore, with the vast hydrogen potential as an alternative to fossil fuels and Brazil's privileged underground storage facilities, this paper proposes the installation of a salt cavern for hydrogen storage (UHS) in the pre-salt fields. This opportunity could put Brazil in a leading position in North and South America, supplying the region and possibly Europe. The investment contemplates the cavern construction up to the operation, thermal effects during cycling, and their impact on cavern integrity. The temperature variation due to the hydrogen injection/discharge cycles is evaluated through a thermodynamic simulator based on the diabatic analytical solution proposed by Ref. [22]. It updates the gas pressure and

Please cite this article as: Dias W et al., Cavern integrity for underground hydrogen storage in the Brazilian pre-salt fields, International Journal of Hydrogen Energy, https://doi.org/10.1016/j.ijhydene.2023.03.292

temperature at each time step (t_{n+1}), considering the previous state (t_n). This solution assumes that the gas density in the cavern is constant at a given time step and that heat diffusion into the salt rock occurs very rapidly. The gas properties are obtained through a link to the REFPROP package, which contains a significant database of gases under different conditions. Thermomechanical models are adopted in the finite element method (FEM) simulations. The results obtained by the thermodynamic simulator are incorporated into the analysis as a boundary condition. Thereby, rock creep considers the temperature variations due to the gas injection/withdrawal, inducing thermal strains/stresses. Pressures are controlled not to overcome the maximum and minimum limits from the reference literature [19,21,23]. All results are compared with a mechanical model to evaluate the contribution of thermal effects. Finally, the permeability change during the cycles is adapted using an empirical relationship that depends on the volumetric strains [24].

Salt rock mechanics

Salt rocks are generated from evaporated seawater deposits. They have very different material behaviors if compared to standard rocks. For instance, the thermal conductivity of salt rocks is about three times higher [25]. Other properties such as fracture strength, self-healing, solubility in water, and sealing capacity due to low porosity and permeability are also relevant to operations. Regarding the unconfined compressive strength (UCS), Fairhurst et al. (1979) [26] tested some salt samples in the Sergipe salt deposit (Brazil). Table 1 reports the strength values.

According to Ref. [27], halite has a low tensile strength (approximately 1.80 MPa), emphasizing how vital temperature control is in engineering projects. For example, excessive cooling may induce high tensile stresses. A relevant characteristic of salt rocks is self-healing [11], defined as the capacity to recover from damage when exposed to sufficient pressures and temperatures. This process can improve the mechanical properties/permeability of damaged rocks and is related to the recrystallization of salt crystals.

In salt rocks, creep plays an essential role. In a general sense, creep is the evolution of plastic deformations over time under conditions of constant stress state and temperature. The higher or lower creep rate relates to material viscosity, temperature, and rock stress state. One of the most important engineering projects related to the creep response of rocks is the WIPP (Waste Isolation Pilot Plant), developed by the US Department of Energy (DOE). The main objective of WIPP is to encapsulate toxic material, taking advantage of salt rock creep. Significant results were achieved in this project, for instance, the development of the multi-mechanism (MD) deformation model [28]. A complete creep process is usually divided into three stages as follows: transient (primary creep), steady-state (secondary creep), and critical stage that precedes damage (accelerative or tertiary creep). A complete creep curve is shown in Fig. 1.

Primary or transient creep corresponds to the blue line of the strain curve. The evolution of the elastic strains is the principal characteristic of this stage. After applying differential stresses, the strain rate has a peak (high creep rate) that decreases over time until it reaches a constant value that will identify the beginning of the stationary stage. Secondary or steady-state creep corresponds to the stationary section of the strain curve (green line), so creep strains occur at a constant rate, assuming that the loading and temperature conditions also remain constant. This stage is one of the most observed in the literature focused on the mechanics of salt rocks [29,30]. Tertiary creep or accelerative creep corresponds to the final ascending stage of the strain curve (orange line). It is defined by a high strain rate associated with localized damage, which leads to material rupture. Dilatancy of the material occurs in this stage.

Table 1 – UCS values for salt rocks with different compositions [26].

Mineral	UCS (MPa)
Halite	37.3
Sylvinite	42.3
Carnallite	19.7
Tachyhydrite	3.0

In parallel with creep laws, dilatancy criteria are commonly used to verify the stability and feasibility of engineering projects related to salt rock mechanics. The dilatancy phenomenon is linked to damage, as high volume expansion is associated with micro-fractures and, consequently, loss of material strength and the development of flow paths [31]. According to Ref. [21], the salt cavern walls are in direct contact with the storage material, and access to the cavern is restricted to measuring tools. Therefore, it is essential to guarantee its integrity during the planned lifespan. In this context, dilatancy criteria are relevant, enhancing the safety requirements. The material will exhibit dilatant behavior if a specific dilatancy criterion is exceeded. Thereby, the volumetric expansion is significant, and microcracks will become

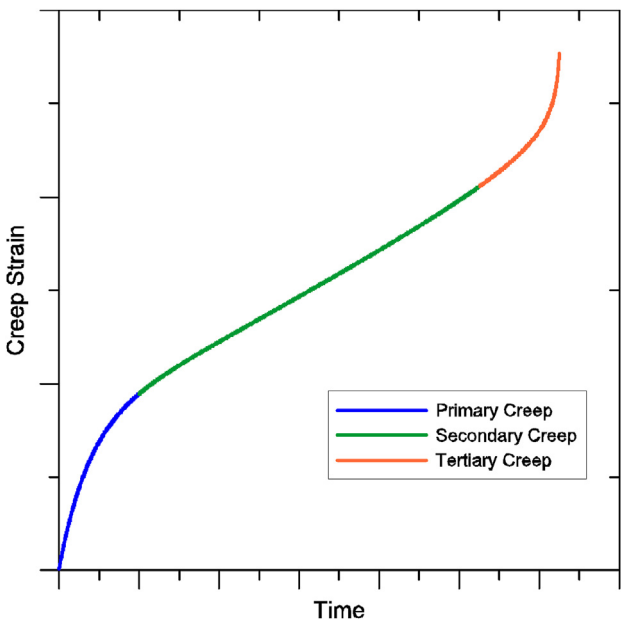

Fig. 1 – Typical creep curve and its corresponding stages.

Please cite this article as: Dias W et al., Cavern integrity for underground hydrogen storage in the Brazilian pre-salt fields, International Journal of Hydrogen Energy, https://doi.org/10.1016/j.ijhydene.2023.03.292

evident. The literature divides these criteria into two main groups: a) strain-based criteria, which consist of defining a threshold for the strains, for example, the norm of the visco-plastic strain or its rate; b) stress-based criteria, which are defined by the stress state [31–36].

Dilatancy boundaries have their basis in laboratory tests, such as triaxial tests. The factor that impacts the dilatancy boundary the most is the stress state. The principal dilatancy stress-based criteria are formulated in terms of the mean stress (σ_m), and the critical deviatoric stress ($\sigma_{d,limit}$) expressed as $\sqrt{3J_2}$, where J_2 is the second invariant of the deviatoric stress tensor [21].

Spiers' boundary [32] originates in experiments with salt cores from the Asse mine. The tests were conducted under a temperature range from 20 to 200 °C, a confinement pressure range from 0 to 50 MPa, and a constant strain rate range from 10^{-7} to 10^{-4} s. The maximum allowable deviatoric stress is a function of the mean stress:

$$\sigma_{d,limit} = (A\sigma_m + B)\sqrt{3} \quad (1)$$

where A = 0.83 and B = 1.9. Even when unconfined ($\sigma_m = 0$), the material remains in the compressive regime. Hunsche (1993) [33] proposed a dilatancy boundary based on uniaxial and triaxial tests from the Asse mine. A quadratic function of the mean stress best fits the experimental data:

$$\sigma_{d,limit} = (C{\sigma_m}^2 + D\sigma_m)3 / \sqrt{2} \quad (2)$$

where C = −0.0168 and D = 0.86. According to Ref. [9], this boundary crosses the mean stress axis at approximately 50 MPa. A modification in the dilatancy boundary was also proposed by replacing the downward trend of the parabola with a rectilinear band of low slope. The equations for the upper and lower limits were presented by Ref. [21], respectively:

$$\sigma_{d,limit} = A_1 e^{C_1\sigma_m} - B_1 e^{D_1\sigma_m} \quad (3)$$

$$\sigma_{d,limit} = A_2 e^{C_2\sigma_m} - B_2 e^{D_2\sigma_m} \quad (4)$$

where A_1 = 25.02, A_2 = 19.06, B_1 = 17.9, B_2 = 19.23, C_1 = 0.004636, C_2 = 0.00562, D_1 = −0.1285 and D_2 = −0.1139. Van Sambeek, Ratigan, and Hansen (1993) [34] performed triaxial tests with WIPP salt samples, leading to the definition of a new boundary. It is one of the most utilized in Brazilian salt rock projects [27,37–40]. The function is expressed by:

$$\sigma_{d,limit} = (0.81\sigma_m)\sqrt{3} \quad (5)$$

DeVries' boundary [36] is based on laboratory tests with salt samples from a formation near Cayuta in New York. It considers the effect of the intermediate stress on rock strength and the mechanical responses for compression/extension due to the Lode angle (+30° for triaxial compression and −30° for triaxial extension). The function is:

$$\sigma_{d,limit} = \left(\frac{E(|3\sigma_m|)^k + F}{\sqrt{3}\cos\theta - G\sin\theta}\right)\sqrt{3} \quad (6)$$

where E = 0.77, F = 1.95, G = 0.524, k = 0.693 and θ is the Lode angle.

Methodology for cavity integrity analysis

Cavern integrity analysis follows a methodology that contemplates cavern geometry, identification of the repository properties, definition of allowable pressures and temperature amplitudes, constitutive model for salt rock, and cyclic operation details.

Cavern geometry, initial stress state, and temperature

Identifying the actual cavern geometry is difficult, as the sonar accuracy is typically 1% when the distance from the cavern axis to the cavern wall is concerned [41]. However, the literature commonly simplifies the cavern shape when the sonar data is unavailable, sometimes adopting a capsular form or circular geometries [14,17,19,21]. This research considered a capsular cavern with the dimensions presented in Ref. [21]. Thus, it has a volume of approximately 2,090,000 m^3 and an area of 94,250 m^2. The initial stress state assumes a representative scenario of the Brazilian pre-salt deep-water environments, consisting of an offshore basin sited in a region where the water depth is approximately 2000 m. The rock formation has a 700 m overburden (from −2000 m to −2700 m depth) followed by 1000 m of salt (halite), where the cavern is hosted. The hypothesis of a significant horizontal continuity throughout the cavern's immediate surroundings is also adopted (salt-bedded region) [21]. The cavern is in the halite layer at −3050 to −3350 m. The slab protection at the top of the cavern is 350 m thick. The isotropic initial stresses ($SV = SH = Sh$) are imposed with null deformations. The specific weight of the overburden is 22.56 kN/m^3 [58], and the salt rock is 21.30 kN/m^3 [27,42]. The temperature is evaluated with the following geothermal gradients: 30 °C/km for the overburden and 12 °C/km for the salt rock [20]. The temperature of the sea bed is 4 °C. Fig. 2 shows the axisymmetric model and the in-situ vertical stress and temperature inside the salt rock.

Thermodynamical analysis of hydrogen caverns

Temperature and pressure are essential state variables in thermodynamic analysis and cave modeling. Currently, two approaches take into account the impact of these variables, the adiabatic and the diabatic. The difference between these approaches is that the adiabatic ignores the heat exchange between cavern air and the surrounding rock, leading to more significant temperature and pressure amplitudes than the real ones. The diabatic approach considers heat exchange and can more accurately predict caverns' thermodynamic response [14,22]. The cavern is regarded as a control volume system. The gas cyclically flows inside the cavern through the cavern port. Two other premises are adopted: the kinetic and potential energy variations are slight and therefore ignored; hydrogen leakage is precluded due to the salt rock's low permeability.

The equations proposed in the present work for the thermodynamic analysis in caves applied to the control volume follows.

Please cite this article as: Dias W et al., Cavern integrity for underground hydrogen storage in the Brazilian pre-salt fields, International Journal of Hydrogen Energy, https://doi.org/10.1016/j.ijhydene.2023.03.292

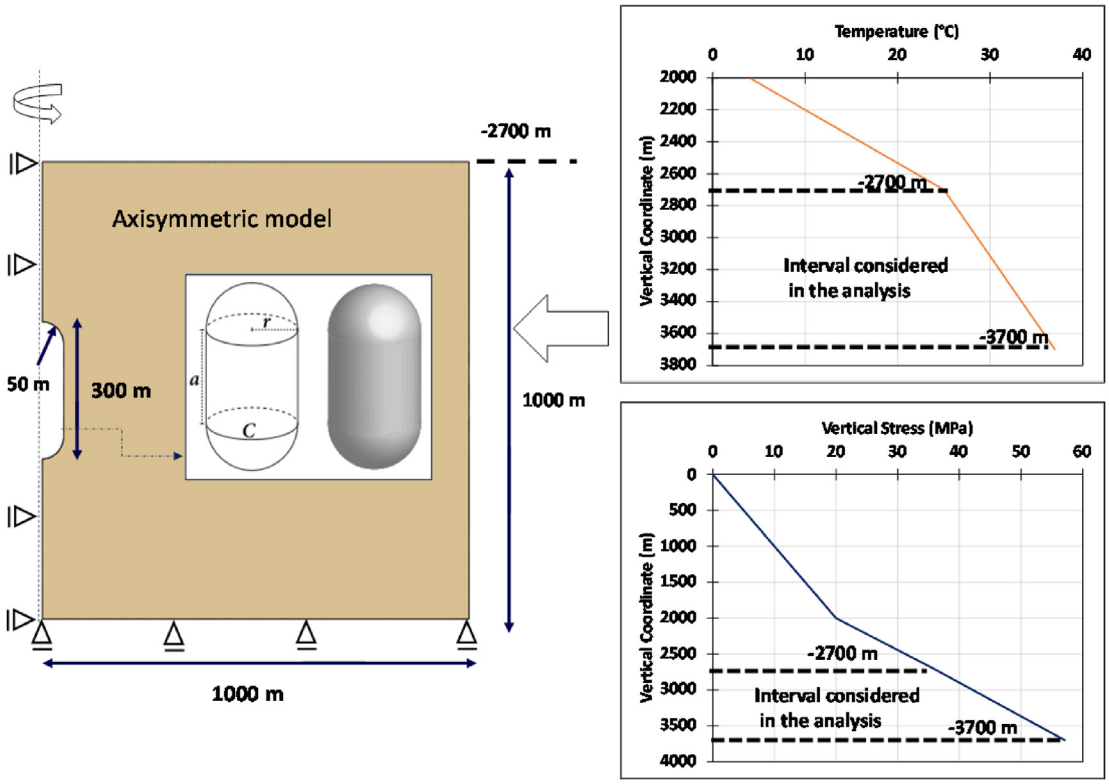

Fig. 2 – Axisymmetric model of the salt cavern with in-situ vertical stress and temperature.

Mass conservation equation

$$V\frac{d\rho}{dt} = \dot{m}_i(t) + \dot{m}_e(t) \tag{7}$$

where ρ is the gas density, $\dot{m}_i(t)$ and $\dot{m}_e(t)$ are a function of the injected and withdrawn air mass flow rate. The gas density in the cavern is constant at a given time step, and heat diffusion into the salt rock occurs fast. Likewise, leakages are ignored when the surrounding rock is salt or a low-permeability rock [22].

Energy conservation equation

$$V\rho c_v\frac{dT}{dt} = \dot{m}_i(t)\left(h_i - h + ZRT - \rho\frac{\partial u}{\partial \rho}\bigg|_T\right) + \dot{m}_e(t)\left(ZRT - \rho\frac{\partial u}{\partial \rho}\bigg|_T\right) + \dot{Q} \tag{8}$$

V is the cavern volume, c_v is the constant volume-specific heat, h_i is the specific enthalpy of injected air, h is the specific enthalpy of the air, u is the specific internal energy of air, Z is the air compressibility, R is the specific air constant, and $\dot{Q}$ is the convective heat transfer rate.

Generalized gas state equation

$$p = Z\rho RT \tag{9}$$

Heat convection equation at cavern walls

$$\dot{Q} = h_c A_c (T_{RW} - T) \tag{10}$$

h_c represents the heat transfer coefficient, A_c is the cavern wall surface area, and T_{RW} is the cavern wall surface temperature.

Heat conduction equation in the surrounding rock

$$\rho_R c_{pR}\frac{dT_R}{dt} = \frac{1}{r}\frac{\partial}{\partial r}\left(k_R r\frac{\partial T_R}{\partial r}\right) \tag{11}$$

where ρ_R is the rock density, c_{pR} represents specific heat at constant pressure, k_R stands for thermal conductivity, and T_R

Table 2 – Data for the thermodynamical analysis [14,22,43].

Properties	Units	Values
Density	$kg.m^{-3}$	2040
Thermal Conductivity	$Wm^{-1}K^{-1}$	7
Thermal expansion coefficient	K^{-1}	4×10^{-5}
Specific heat capacity	$Jkg^{-1}K^{-1}$	880
Heat transfer coefficient	$Wm^{-2}K^{-1}$	1.2
Cavern surface area	m^2	94,250
Cavern volume	m^3	2,090,000
Injection temperature	K	333

Please cite this article as: Dias W et al., Cavern integrity for underground hydrogen storage in the Brazilian pre-salt fields, International Journal of Hydrogen Energy, https://doi.org/10.1016/j.ijhydene.2023.03.292

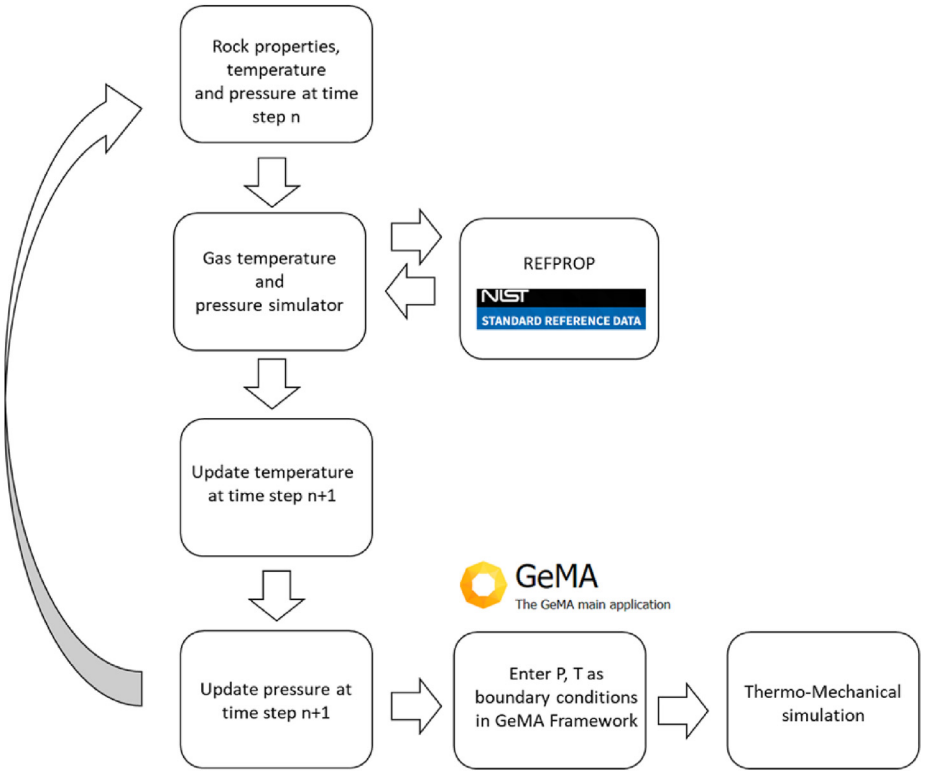

Fig. 3 – Analysis flowchart.

is the temperature. The following boundary conditions are adopted:

$$\begin{aligned} &r = R_w, -k_R r\frac{\partial T_R}{\partial r} = h_c(T - T_{RW}) \\ &r \to \infty, T_R = T_0 \end{aligned} \tag{12}$$

The control of the air mass flow in the cavern is defined as positive; otherwise, it is negative.

Calculating the air temperature and pressure requires the simultaneous solution of the above equations, which implies complex numerical computations [22]. Considering the assumptions made and that a constant average value can represent the cavern air density (ρ_{AV}), when the ratio of injected air mass to the initial cavern air mass m_r is small, we have:

$$V\rho_{AV}c_v\frac{dT}{dt} = \dot{m}_i(t)(h_i - h + RT) + \dot{m}_e(t)RT + h_cA_c(T_{RW} - T) \tag{13}$$

Table 3 – Properties for the Brazilian halite [27].

Parameter	Units	Value
Young's modulus (E)	GPa	25.37
Poisson's ratio (ν)	–	0.36
Thermal activation energy (Q)	J/mol	50,160
Universal gas constant (R)	J/mol.K	8.314
Threshold creep rate ($\dot{\varepsilon}_0$)	(h^{-1})	1.88×10^{-6}
Threshold deviatoric stress (σ_0)	MPa	9.91
Threshold temperature (T_0)	K	359.15
Stress power for dislocation creep (n_1)	–	3.36
Stress power for steady-state cracking (n_2)	–	7.55

In a given period (charging, discharging, or storage), the value of the function $\dot{m}_i(t)$ is constant (either m_i or 0) and $\dot{m}_e(t)$ is also constant (either m_e or 0). This leads to

$$T = (T_0 + \alpha)e^{\beta(t-t_0)} - \alpha \tag{14}$$

where α and β are charging and discharging coefficients, respectively. They are calculated according to Eq. (15) with the air temperature T_i updated at each time step, and the air pressure (or other gas) follows from Eq. (9).

$$\alpha = \begin{cases} \dfrac{m_i c_p T_i + h_c A_c T_{RW}}{m_i(R - c_p) - h_c A_c}, t_0 \le t \le t_1 \text{ (charging period)} \\ -T_{RW}, t_1 < t \le t_2 \text{ (storage period)} \\ \dfrac{h_c A_c T_{RW}}{m_e R - h_c A_c}, t_2 < t \le t_3 \text{ (discharging period)} \\ -T_{RW}, t_3 < t \le t_4 \text{ (storage period)} \end{cases} \tag{15}$$

$$\beta = \begin{cases} \dfrac{-h_c A_c}{V\rho_{AV}c_v}, t_1 < t \le t_2 \text{ (storage period)} \\ \dfrac{m_e R - h_c A_c}{V\rho_{AV}c_v}, t_2 < t \le t_3 \text{ (discharging period)} \\ \dfrac{-h_c A_c}{V\rho_{AV}c_v}, t_3 < t \le t_4 \text{ (storage period)} \end{cases}$$

The present work calculated the thermodynamic and hydrogen transport properties using the REFPROP package (NIST Standard Reference Database 23, Version 9.0). The gas properties are obtained through a link with REFPROP, which updates the pressure and temperature at each increment. The

Please cite this article as: Dias W et al., Cavern integrity for underground hydrogen storage in the Brazilian pre-salt fields, International Journal of Hydrogen Energy, https://doi.org/10.1016/j.ijhydene.2023.03.292

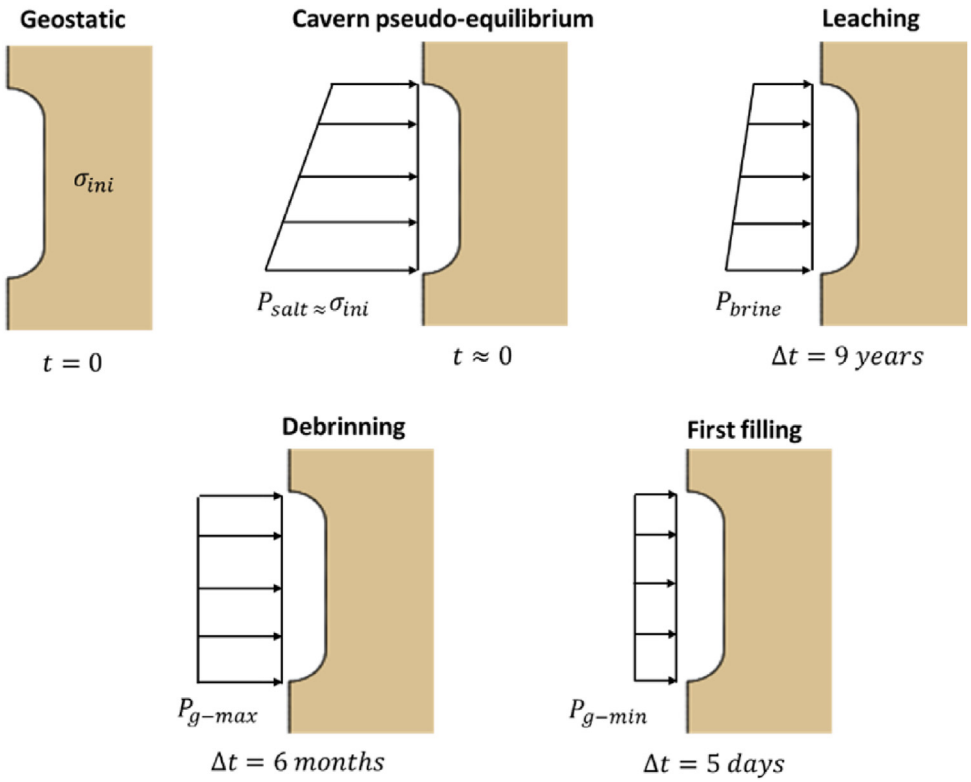

Fig. 4 – Simulation steps and their assumptions.

material properties of salt rock and parameters for the thermodynamic analysis are presented in Table 2. The literature sets a pressure range of 30–90% of the lithostatic stress at the top of the cavern [18,20,21]. In this study, the gas pressure will be controlled by the lower limit of 30% and the upper limit of 80%.

The inputs from the thermodynamical simulator were fed into the GeMA Framework [44], an in-house multiphysics simulator based on the finite element method. Fig. 3 shows the simulation procedure.

Regarding the thermo-mechanical coupling, the incremental total strain $\Delta\varepsilon$ is given by:

$$\Delta\boldsymbol{\varepsilon} = \Delta\boldsymbol{\varepsilon}_m + \Delta\boldsymbol{\varepsilon}_T \tag{16}$$

where $\Delta\boldsymbol{\varepsilon}_m$ represents the increment of mechanical strain, $\Delta\boldsymbol{\varepsilon}_T = \boldsymbol{m}\alpha_T\Delta T$ is the increment of thermal strain, α_T stands for the thermal expansion coefficient and $\boldsymbol{m} = \{1\,1\,1\,0\,0\,0\}$. The soil constitutive behavior considering thermal effects results in:

$$\Delta\boldsymbol{\sigma} = \boldsymbol{D}\Delta\boldsymbol{\varepsilon} - \boldsymbol{D}\boldsymbol{m}\alpha_T\Delta T \tag{17}$$

$\Delta\boldsymbol{\sigma}$ is the increment of total stress. The last term on the right-hand side of Eq. (17) represents the change in total stress induced by temperature variation, which is the thermal effect on the mechanical equilibrium. Following the standard FEM procedure, the equilibrium equation for a coupled thermo-mechanical behavior of the soil results in:

$$\boldsymbol{K}_G\Delta\boldsymbol{u} - \boldsymbol{M}_G\Delta\boldsymbol{T} = \Delta\boldsymbol{R}_G \tag{18}$$

$\boldsymbol{K}_G$ represents mechanical stiffness matrix, $\boldsymbol{M}_G$ is the TM coupling term, and $\Delta\boldsymbol{R}_G$ is the residual force vector.

$$\boldsymbol{K}_G = \sum_{i=1}^{N}\left(\int_{\Omega}\boldsymbol{B}^T\boldsymbol{D}\boldsymbol{B}d\Omega\right)_i \tag{19}$$

$$\boldsymbol{M}_G = \sum_{i=1}^{N}\left(\int_{\Omega}\boldsymbol{B}^T\boldsymbol{D}\boldsymbol{m}\boldsymbol{N}_T d\Omega\right)_i \tag{20}$$

where $\boldsymbol{B}$ is the matrix that relates the nodal displacement and mechanical strains, $\boldsymbol{N}_T$ is the vector containing shape functions to interpolate the temperature field. Neglecting radiation and the mechanical effect on the thermal system, the governing equation of heat transfer in soils follows the law of energy conservation:

$$\rho C_p\Delta T = \nabla.(k_T\nabla T) + G \tag{21}$$

Table 4 – Case studies adopted in the numerical simulations.

Case study	Description
1	80-day cycle – Mechanical only
2	80-day cycle – Thermo-mechanical (TM)
3	20-day cycle – TM
4	20-day cycle with reduced pressure - TM

Please cite this article as: Dias W et al., Cavern integrity for underground hydrogen storage in the Brazilian pre-salt fields, International Journal of Hydrogen Energy, https://doi.org/10.1016/j.ijhydene.2023.03.292

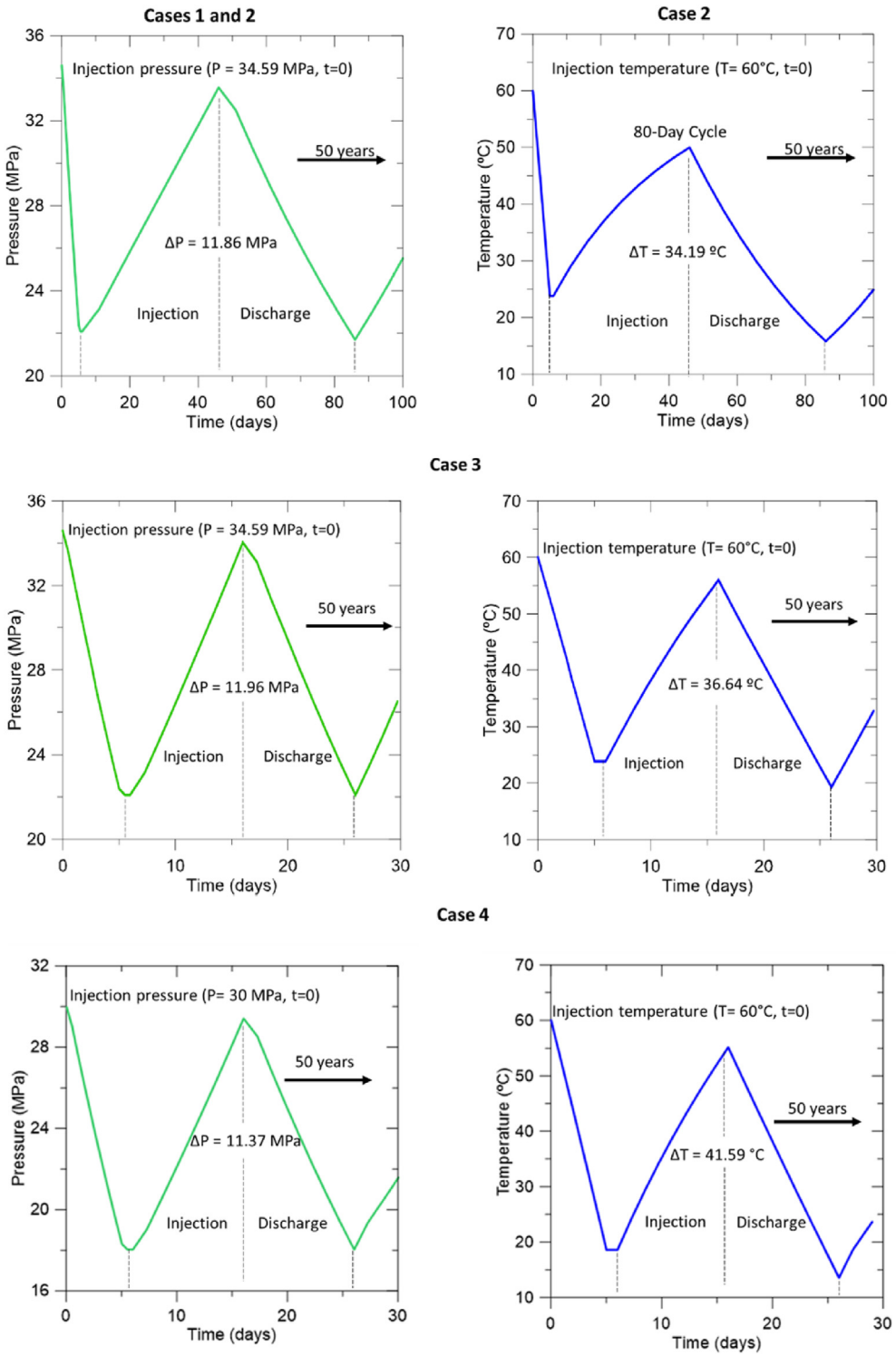

Fig. 5 – Gas pressure and temperature for cases 1 to 4.

k_T is the thermal conductivity, ρ is the soil density, C_p represents the specific heat capacity, and G indicates the heat generation rate. Applying the standard Galerkin method, the finite element equation governing the heat transfer can be assembled in terms of global matrices as:

$$\mathbf{C}_G \partial \mathbf{T} / \partial \mathbf{t} + \mathbf{\Phi}_G \Delta \mathbf{T} = \mathbf{Q}_G \tag{22}$$

where $\mathbf{C}_G$ represents the thermal expansion matrix, $\mathbf{\Phi}_G$ is the conductivity and advection capacity matrix and $\mathbf{Q}_G$ stands for the heat source or sink matrix.

Please cite this article as: Dias W et al., Cavern integrity for underground hydrogen storage in the Brazilian pre-salt fields, International Journal of Hydrogen Energy, https://doi.org/10.1016/j.ijhydene.2023.03.292

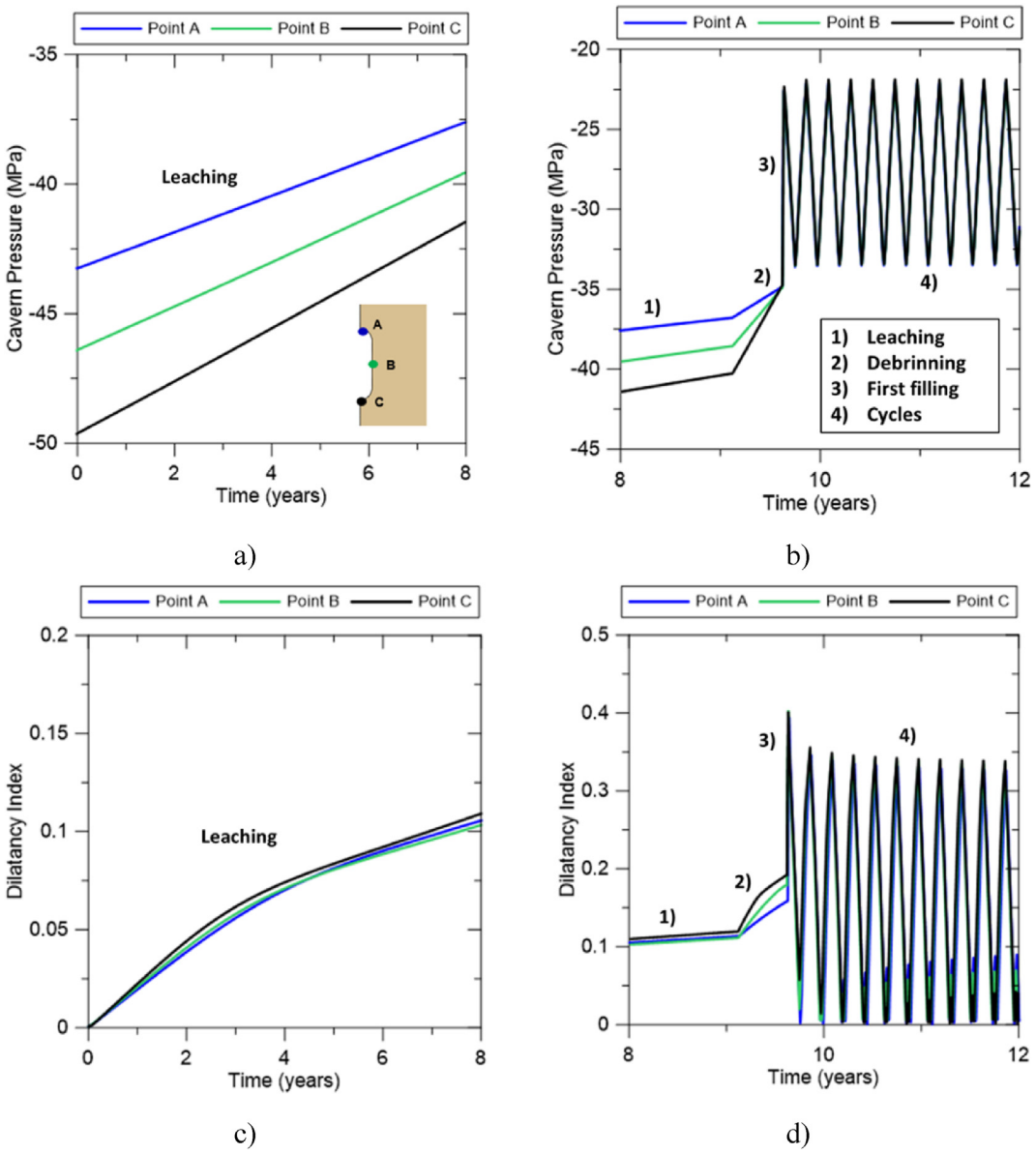

Fig. 6 – a) Cavern pressure during the leaching stage; b) Cavern pressure during the subsequent stages; c) Dilatancy index during the leaching stage; d) Dilatancy index during the subsequent stages.

$$\mathbf{\Phi}_G = \sum_{i=1}^{N} \left(\int_{\Omega} \mathbf{B}_T^T \mathbf{k}_T \mathbf{B}_T d\Omega + \int_{\Gamma} h \mathbf{N}_T^T \mathbf{N}_T d\Gamma \right)_i \tag{23}$$

$$\mathbf{C}_G = \sum_{i=1}^{N} \left(\int_{\Omega} \rho C_p \mathbf{N}_T^T \mathbf{N}_T d\Omega \right)_i \tag{24}$$

Here h is the convection coefficient. Assembling Eq. (18) and Eq. (22) gives the coupled TM equation system:

$$\begin{bmatrix} \mathbf{0} & \mathbf{0} \\ \mathbf{0} & \mathbf{C}_G \end{bmatrix} \begin{Bmatrix} \partial \mathbf{u}/\partial t \\ \partial \mathbf{T}/\partial t \end{Bmatrix} + \begin{bmatrix} \mathbf{K}_G & -\mathbf{M}_G \\ \mathbf{0} & \mathbf{\Phi}_G \end{bmatrix} \begin{Bmatrix} \Delta \mathbf{u} \\ \Delta \mathbf{T} \end{Bmatrix} = \begin{Bmatrix} \Delta \mathbf{R}_G \\ \mathbf{Q}_G \end{Bmatrix} \tag{25}$$

Constitutive model for salt

This research adopts the Double-Mechanism (DM) creep model for the analysis. According to Ref. [38], the DM simplifies the Multi-mechanism (MM) model and considers the secondary creep stage. The formulation for this constitutive model is:

$$\dot{\varepsilon} = \dot{\varepsilon}_0 \left(\frac{\sigma_{ef}}{\sigma_0} \right)^n e^{\left(\frac{Q}{RT_0} - \frac{Q}{RT} \right)} \tag{26}$$

where $\dot{\varepsilon}$ is the strain rate due to creep at steady-state, $\dot{\varepsilon}_0$ is the reference strain rate due to creep (steady-state), T_0 stands for the reference absolute temperature, T is the temperature of

Please cite this article as: Dias W et al., Cavern integrity for underground hydrogen storage in the Brazilian pre-salt fields, International Journal of Hydrogen Energy, https://doi.org/10.1016/j.ijhydene.2023.03.292

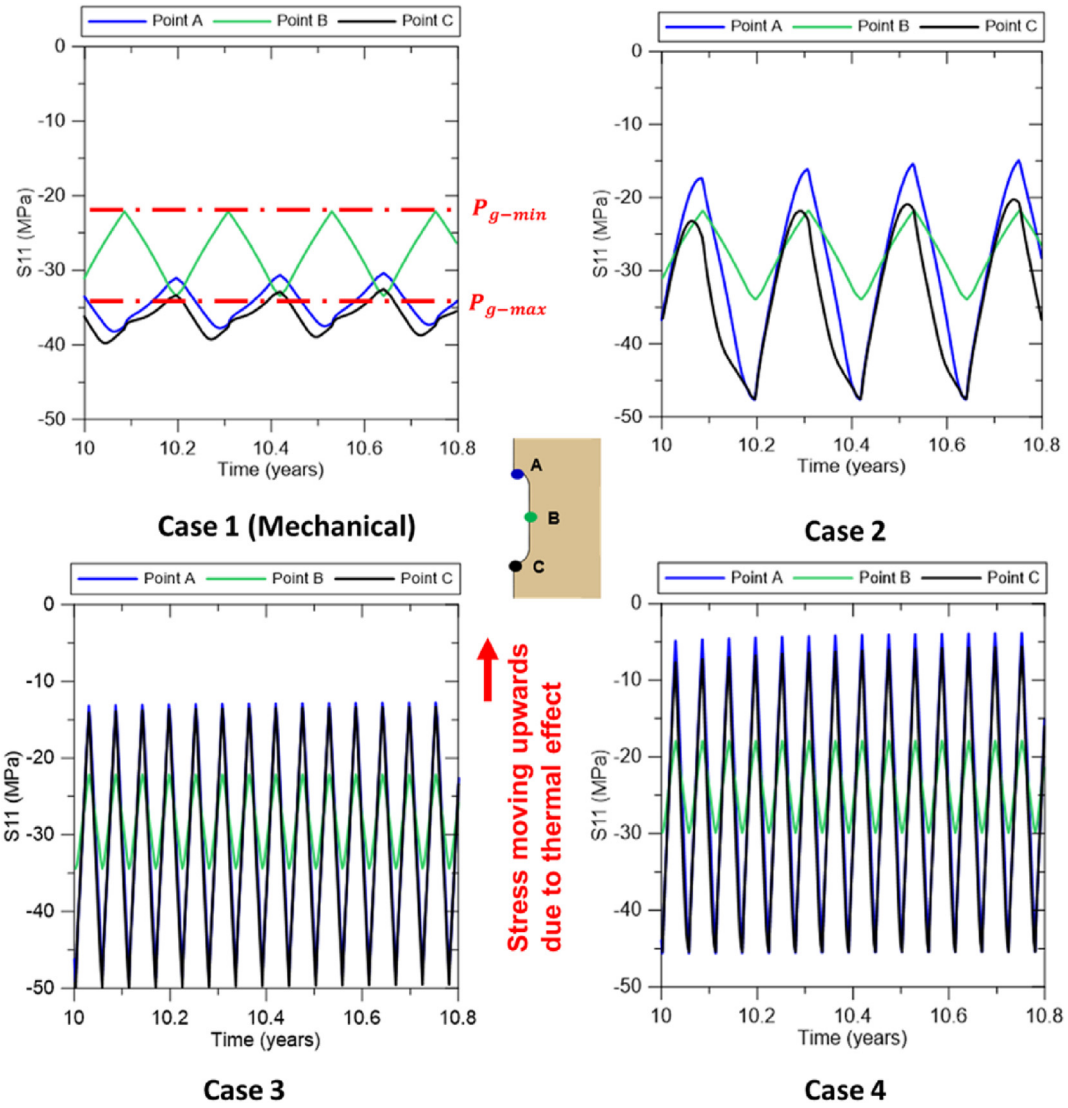

Fig. 7 – Stresses in the x-direction for all the case studies.

the rock, σ_{ef} is the effective creep stress, σ_0 represents the reference effective stress, n is the stress exponent, R is related to the universal gas constant, and Q is the thermal activation energy. The material parameters have been calibrated by [53] and are listed in Table 3.

Regarding dilatancy, this research selected the boundary proposed by Ref. [34]. It is one of the most utilized in Brazilian salt rock projects [27,37,39,40]. To evaluate if dilatancy occurs, we propose a dilatancy index (DI), the ratio between the von Mises equivalent stress obtained from the simulations (σ_d) and the maximum deviatoric stress according to the dilatancy boundary ($\sigma_{d-Sambeek}$). Thus:

$$DI = \frac{\sigma_d}{\sigma_{d-Sambeek}} \tag{27}$$

If the index achieves 1.0, the current stress state reaches the dilatancy boundary, and dilatancy occurs. For cavern safety, keeping *DI* below 1.0 is recommended.

Permeability measurement

The salt rock's low permeability and self-healing features are important to assure cavern safety and tightness. According to Ref. [3], hydrogen leakage and loss are common and severe due to hydrogen's lower density, viscosity, and molecule size. From laboratory measurements conducted by Ref. [24], salt permeability was evaluated as 10^{-20} m^2 or less. However, if dilatancy occurs, permeability is expected to increase, and the sealing capacity of the rock may be compromised. Studies to predict the evolution of salt rock permeability have been conducted by Refs. [9,24,45,46]. Here, we will adopt the criterion proposed by Peach [24], where the permeability is expressed as a power function of the volumetric strains, and the empirical parameters are $\alpha = 2.13\text{x}10^{-8}$ and $\beta = 3.0$:

$$k = \alpha \varepsilon_{vol}^{\beta} \tag{28}$$

Please cite this article as: Dias W et al., Cavern integrity for underground hydrogen storage in the Brazilian pre-salt fields, International Journal of Hydrogen Energy, https://doi.org/10.1016/j.ijhydene.2023.03.292

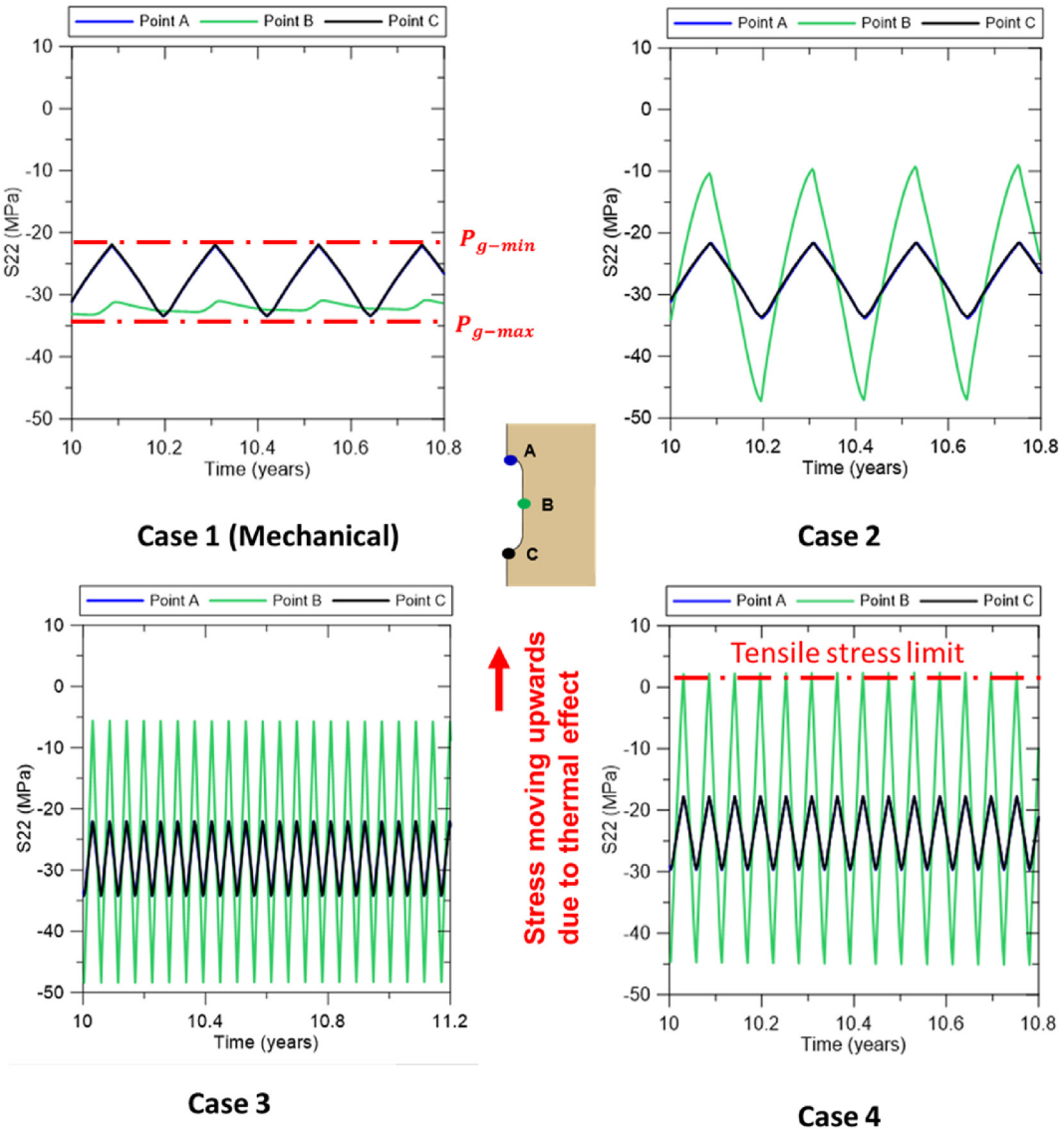

Fig. 8 – Stresses in the y-direction for all the case studies.

The permeability measured in this study refers only to salt rock damage without considering further interaction with the medium, such as dissolution. The gas/rock interaction and how it affects the rock's mechanical and hydraulic properties requires considering coupled hydromechanical or chemical effects.

Steps of cavern construction

Cavern construction will encompass the following stages: a) geostatic equilibrium, b) leaching, c) debrinning, d) first filling, and e) cyclic operation. In geostatic equilibrium, the model remains with the initial stress and temperature conditions presented in section 3.2. The cavern wall has an equivalent fluid pressure ($P_{salt} = 21.30\,kN/m^3$) to maintain the pre-existing stress state (σ_{ini}) and assure no deviatoric stresses rise. In the sequence, the leaching step corresponds to the salt cavern excavation, injection of fresh water, and the formation of a mixture (brine). The unit weight adopted in the salt-equivalent fluid pressure (P_{salt}) is reduced from 21.30 kN/m^3 (salt) to 12 kN/m^3 (brine) over time to represent a realistic solution mining rate. From Ref. [47], we have an average dissolution rate of 26.5 m^3/h, which results in approximately nine years to complete the process.

The next step is debrinning, when gas injection into the salt cavern begins, replacing the existing brine. The brine hydrostatic load (P_{brine}) turns into a uniform load (P_{g-max}) when the process is completed. This stage is less time-consuming and was assumed to take six months [17,21]. The last step is the first filling, which corresponds to a gas pressure reduction from the maximum pressure (P_{g-max}) to the minimum pressure (P_{g-min}). It takes five days [47] to finish this process. The limits P_{g-max} and P_{g-min} are obtained from the pressure curve. Temperature variation will only occur in the first filling stage

Please cite this article as: Dias W et al., Cavern integrity for underground hydrogen storage in the Brazilian pre-salt fields, International Journal of Hydrogen Energy, https://doi.org/10.1016/j.ijhydene.2023.03.292

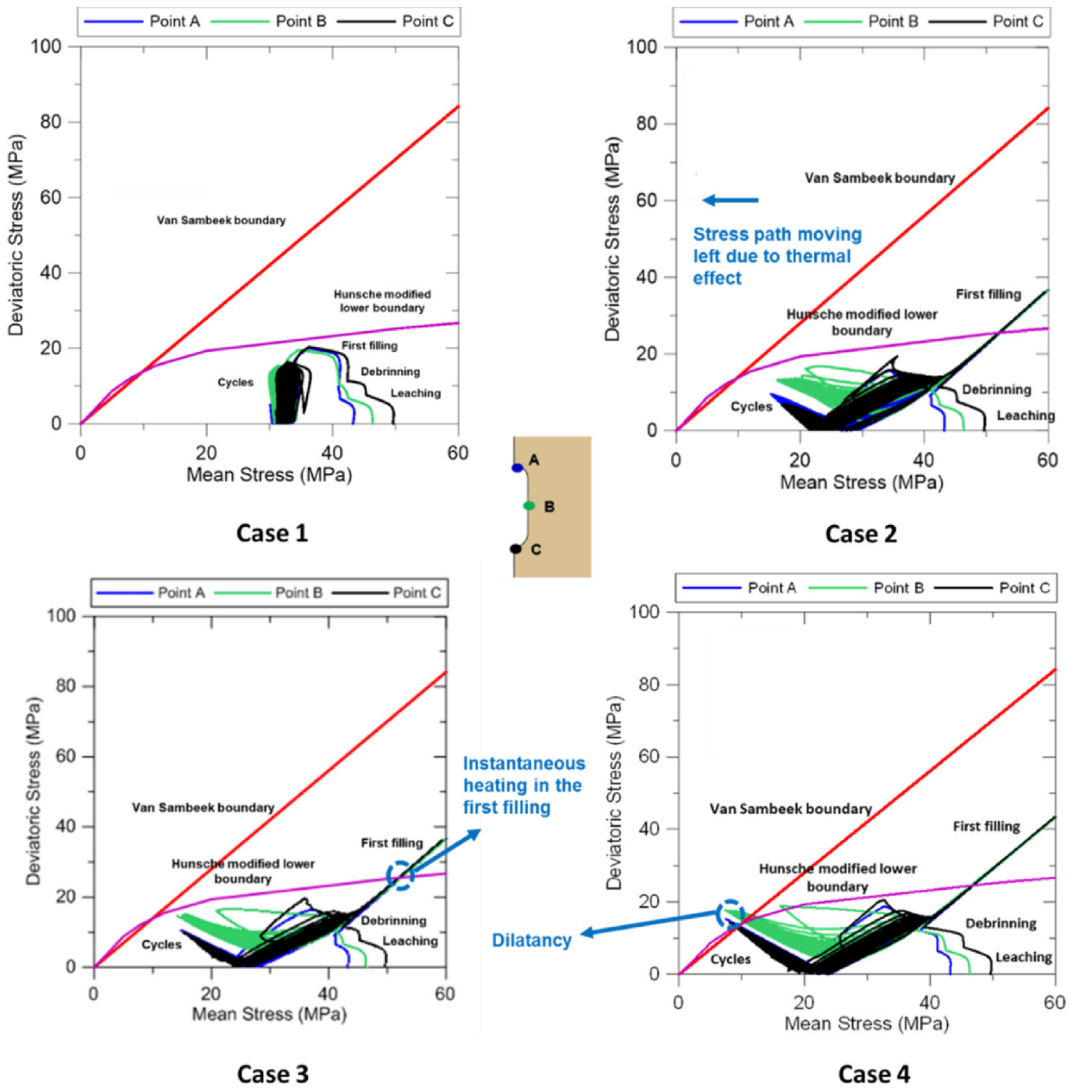

Fig. 9 – Stress trajectory p x q for all the case studies.

due to cavern depressurization. Thereby, the simulation is mechanical until this stage. Fig. 4 shows a schematic representation of the simulation steps a) to d) and their assumptions.

Regarding the cyclic loading, it is expected to last 50 years. Thus, the total time of simulation is approximately 60 years. We selected four case studies, summarized in Table 4.

The cycle duration was determined to cover long and short supply periods. In Brazil's first years of technology implementation, case 2 is expected to be dominant. However, the country can soon assume leadership in hydrogen storage with the support of the expertise acquired from the exploration into ultra-deep waters and the demand for renewable energies in South America. In this scenario, short periods will be a reality, and cases 3 and 4 require investigation. Fig. 5 shows the gas pressure and temperature for the four case studies.

Case 1. is a mechanical analysis used as a reference for case 2, a TM simulation with the same cycle time to evaluate how temperature affects cavern creep and its safety. Case 3 represents a short cycle (four times shorter than case 2). Cavern closure is expected to increase, and the safety criteria will become more relevant. In case 4, the injection pressure drops from 80% to approximately 70% of the lithostatic pressure at the cavern top. The objective of this case study is to evaluate the impact of pressure reduction on the temperature amplitudes and, consequently, the rock integrity.

Results and discussion

This section presents the numerical results of cavern integrity obtained from the four case studies. For better understanding, we monitor stresses, dilatancy index, permeability, and displacements at three cavern points (A, B, and C). We emphasize that the simulations are purely mechanical until the first filling stage. Thus, Fig. 6 exhibits the results for case 1, considering only the mechanical analysis.

Please cite this article as: Dias W et al., Cavern integrity for underground hydrogen storage in the Brazilian pre-salt fields, International Journal of Hydrogen Energy, https://doi.org/10.1016/j.ijhydene.2023.03.292

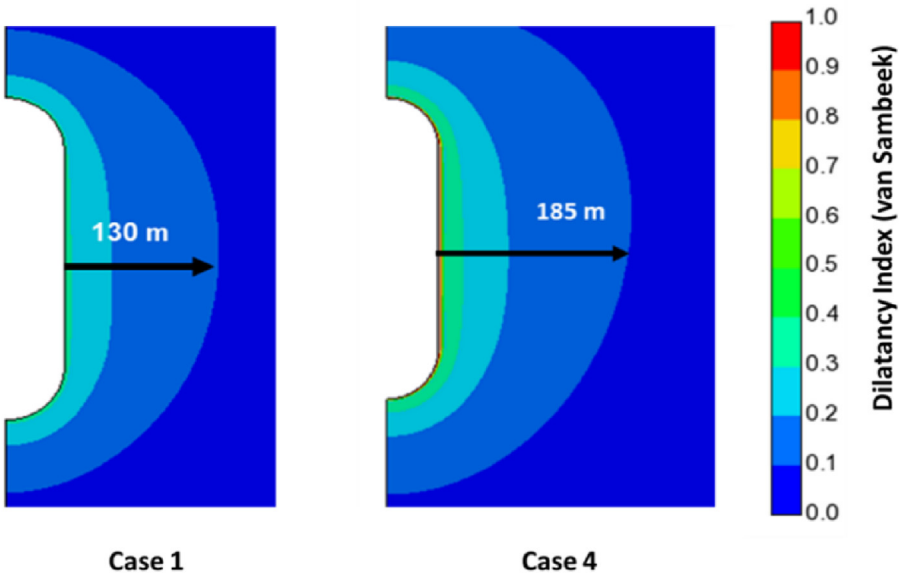

Fig. 10 – Comparison of *DI* disturbed zones between cases 1 and 4.

The stresses in *the* x-direction (S11) for points A and C follow the cavern pressure and vary according to the simulation stage (geostatic, leaching, debrinning, first filling, and cycles). At point B, the same happens to the stresses in the y-direction (S22). Cavern construction (leaching stage) did not significantly affect rock integrity once the dilatancy index remained low. On the other hand, the first filling seems more critical, as the cavern suffers high depressurization in a short period. In this stage, the dilatancy index achieves approximately 0.4. However, rock integrity is still assured.

Regarding the cyclic operation, the stresses in the x-direction (S11) are shown in Fig. 7. Stresses increase in points A and C due to the thermal effect. While in the mechanical analysis, stresses in x are approximately −30 MPa, during the TM analyses (cases 2 to 4), stresses rise, moving towards tension. At point B, the stress value is in the range P_{g-max} to P_{g-min} (output from the thermodynamical simulator). We also observed the influence of the cycle duration; the longer the cycle, the smaller the tendency of tensile stresses to occur. Thus, cases 3 and 4 present a higher stress variation than case 2. In case 4, despite having the same cycle duration as case 3, the reduction of the injection pressure turned the results even more critical.

The stresses in the y-direction are shown in Fig. 8. Points A and C have equal stresses that vary from P_{g-max} to P_{g-min}. The thermal effect was more significant at point B, as tensile stresses occurred during case 4 simulations. However, for cases 2 and 3, the thermal effect is less critical. It happens because the cavern depth was sufficient to avoid tension, as the in-situ confining stresses increased in depth. However, in case 4, we noticed a tensile stress of 2.4 MPa at point B, above the halite tensile strength limit of approximately 1.80 MPa [27]. Furthermore, the stress state violated the zero-tensile stress criterion, and cavern integrity was not assured. This example confirmed the expectation of high-temperature amplitude ($\Delta T = 41.59\ ^{\circ}C$) inducing tensile stresses. We point out that a slight reduction in the injection pressure (10%) drastically changed the loading scenario, warning the operators of the importance of a good assessment of the initial stress condition.

Table 5 provides the stress increase (%) in the x and y directions, taking case 4 as a reference.

Case 4 showed a significant stress increase in the vertical direction once the percentual overcame 100% compared to all the previous examples. To avoid damage in the salt cavern, reducing the frequency of the storage cycles may be a viable alternative [14].

Regarding the p-q stress path, the numerical results are analyzed considering two dilatancy boundaries. The first was proposed by van Sambeek et al. [34] – red line and the second is the modified Hunsche lower boundary (more critical) [33] – pink line, as shown in Fig. 9.

Table 5 – Comparison of horizontal S_{11} and vertical S_{22} stresses in case 4 against cases 1 to 3.

Case study	% S_{11} increase (x direction)	% S_{22} increase (y direction)
01	83%	108%
02	71%	124%
03	64%	148%

Table 6 – Permeability summary after the simulations.

Case study	Maximum permeability (m^2)
01	5×10^{-18}
02	1.7×10^{-16}
03	3.7×10^{-16}
04	3.5×10^{-16}

Please cite this article as: Dias W et al., Cavern integrity for underground hydrogen storage in the Brazilian pre-salt fields, International Journal of Hydrogen Energy, https://doi.org/10.1016/j.ijhydene.2023.03.292

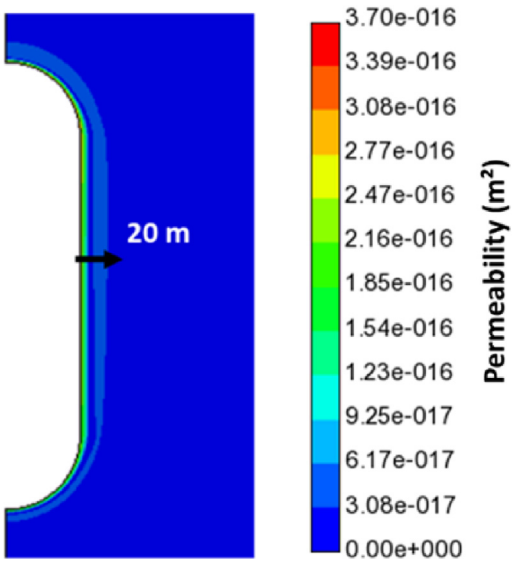

Fig. 11 – Permeability changes in the host rock.

Before the first filling, the temperature inside the cavern and the salt layer coincide; consequently, there is no thermal contribution. Afterward, we observe successive peaks during the stress path, corresponding to each simulation step. The stress path remains inside the compression domain for mechanical (case 1) and TM analyses (cases 2 and 3). However, all TM cases violate Hunsche's boundary during the first filling stage. This peak stress occurs due to the high-temperature gas injection (60 °C), while the salt layer has an average temperature of 30 °C. The sudden heating raises the stresses abruptly. To mitigate this effect, gradual heating of the cavern wall is recommended. In the cyclic loads, the stress path moved fast to the left. Dilatancy was observed in case 4 for both boundaries at all monitored points (A, B, and C), indicating that injection pressure reduction is a warning of cavern integrity loss. Cavern damage can compromise the permeability of the salt layer, and gas migration into the surrounding salt rock is inevitable.

We point out that the current constitutive model does not evaluate the interaction between the dilatancy and self-healing phenomena. Thus, this is a more conservative approach, as healing can counterbalance damage propagation into the host rock.

As expected, the mechanical analysis (case 1) presented the lowest DI, highlighting the importance of coupled simulations (TM). For instance, the less critical TM analysis (case 2) had a *DI* increase of approximately 57% compared to case 1. On the other hand, in the most critical TM analysis (case 4), *DI* increased by

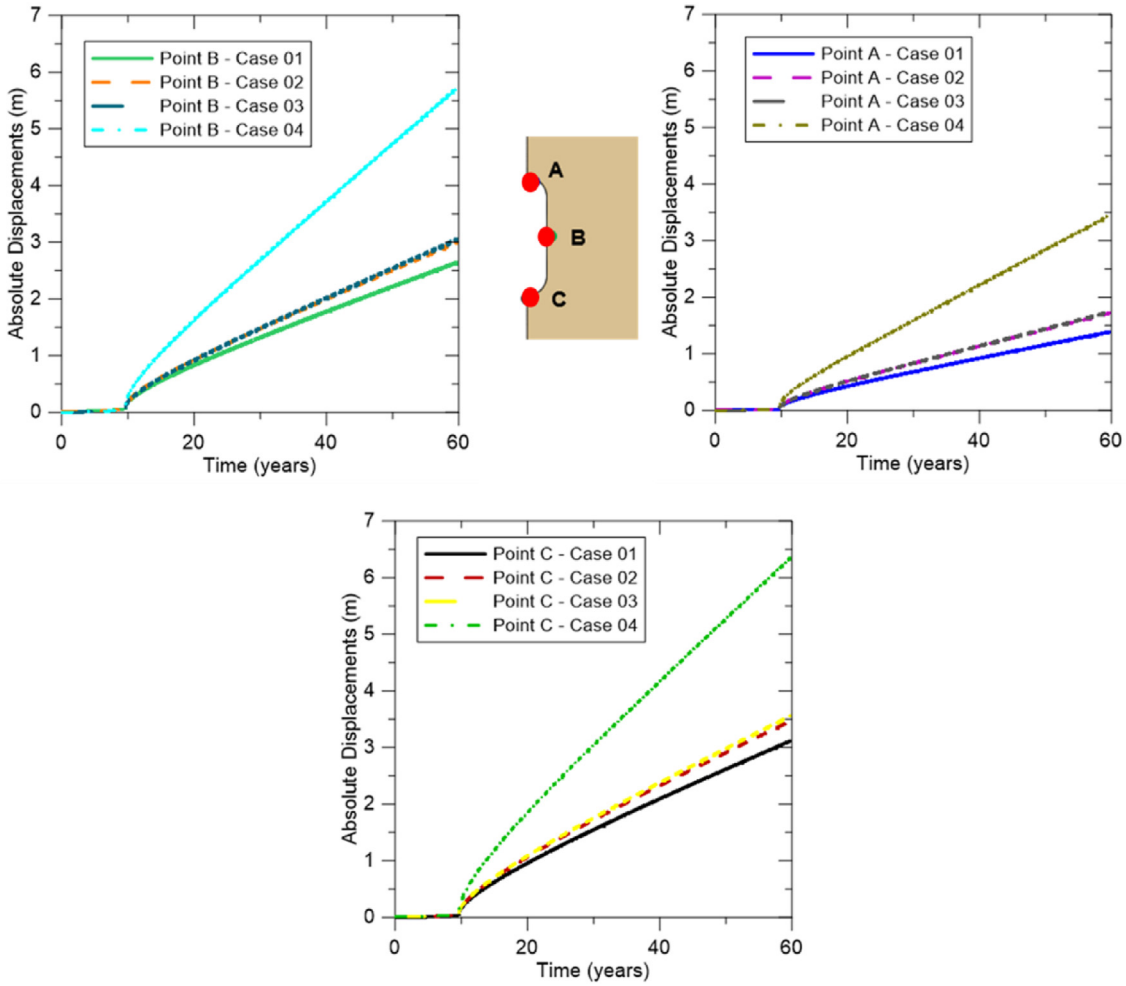

Fig. 12 – Cavern displacements at all the monitored points for all the case studies.

Please cite this article as: Dias W et al., Cavern integrity for underground hydrogen storage in the Brazilian pre-salt fields, International Journal of Hydrogen Energy, https://doi.org/10.1016/j.ijhydene.2023.03.292

185% regarding the same reference. We notice again how the injection pressure affects the results; for example, *DI* in case 4 is approximately 30% higher than in case 3.

Regarding the *DI* zone of influence inside the salt rock, the mechanical simulation showed an affected region of approximately 130 m measured radially from the cavern wall. However, we noticed a further advance of more than 50 m into the host rock for the TM simulation in case 4 (the most critical). In the zone where *DI* equals 1.0, the damage is restricted to the cavern wall. Fig. 10 exhibits a comparison between cases 1 and 4.

Regarding permeability, it increased approximately 500 times (from 10^{-20} to 5×10^{-18}) in case 1. However, it remains low, and cavern tightness is still assured. During the TM simulations, the potential for leakage was verified. For instance, in case 2, which has the most extended cycle and less heating or cooling, the maximum permeability was 3.5×10^{-16}. It is 70 times higher than case 1.

As expected, the most critical cases are 3 and 4, when the cycles happen fast. However, the permeability in case 3 is slightly higher than in case 4, even with the reduced injection pressure. The criterion adopted to measure permeability in terms of the volumetric strains is highly influenced by cavern heating. In the TM analyses, we notice that cases 3 and 4 reach similar temperatures, with a more pronounced effect in the cooling stage (cavern depressurization) for case 4. Table 6 presents the maximum permeability obtained in all simulations.

In case 3, the initial permeability of the host rock is affected at a distance of approximately 20 m, as shown in Fig. 11. Since problems involving hydrogen leakage are frequent [8], a hydraulic investigation may be necessary to evaluate better how the gas propagates into the host rock.

Finally, Fig. 12 shows the cavern displacements for all cases. Results are plotted for each monitored point. Cavern creep closure was expressive at point C. As already observed, the mechanical analysis (case 1) presented the lowest displacements. However, compared to all TM simulations, it makes evident how the temperature accelerates closure and, consequently, volume losses, an undesirable effect [14]. According to Ref. [17], when the volume decreases, the storage capacity of the cavern reduces, affecting the serviceability of the whole storage system. The volume reduction also affects gas thermodynamics, turning the process even more complex to be realistically represented [22]. In case 4, displacements were above 6 m for points B and C. It is almost twice that of case 3 with the same cycle duration. The injection pressure is a warning to operators and must be constantly monitored. Comparing TM cases with the same injection pressure (cases 2 and 3), we observed that the cycle frequencies had a minor influence on the displacements, a similar effect evidenced by Ref. [14].

Conclusions

This work discusses the potential for hydrogen storage in salt caverns in pre-salt fields. The most critical aspects of salt cavern simulations are assessed: a) site selection, b) identification of the repository properties, c) definition of allowable pressures and temperature amplitudes, d) constitutive models for creep, and e) safety criteria. Regarding temperature and pressure, studies usually simplify the problem and assume the hypothesis of isothermal conditions in the analysis, focusing only on mechanical behavior (independently of the time cycle). This study demonstrates that the temperature may significantly vary during hydrogen storage and influence the pressure inside the cavern. Thus, the best representation must consider the associated thermodynamics.

The proposed simulation workflow for hydrogen storage considers a thermodynamic simulator based on the diabatic solution of [22], which updates the gas pressure and temperature at each time step (t_{n+1}). The gas properties were evaluated using the REFPROP library, and the estimated cavern pressure and temperature were loaded into the finite element simulator to run the thermomechanical analyses. The double-mechanism creep model governs the mechanical behavior of salt rock. Two dilatancy boundaries were adopted to evaluate the occurrence of salt rock damage [33,34].

A thermomechanical formulation was implemented into the in-house framework GeMA [87], which supported all simulations. Four case studies with different pressure and injection cycles were considered to understand the problem better. Results demonstrated that shorter cycles provoke higher temperature amplitudes and increase damage and leakage risks [14]. The gas injection pressure also plays an important role. A 10% reduction of the injection pressure induced tensile stresses, dilatancy, and significantly increased cavern closure, 100% at point A. The disturbed zone was 185 m into the rock mass in the most critical case. However, the area where dilatancy achieved the limit of 1.0 is restricted to the cavern wall. Temperature amplitudes also affect permeability, which follows Peach's criterion [77] based on a power law of the volumetric strain. The numerical results demonstrate that permeability increases during TM simulations. However, there is a gap in the literature related to the required permeability to guarantee cavern tightness.

Finally, the Brazilian expertise acquired from exploring wells in the pre-salt fields is a differential towards making this challenging project viable, as operations in ultra-depth waters require advanced engineering techniques and simulations. The TM simulations demonstrated that temperature control is important to guarantee rock integrity and avoid possible gas leakages into the host rock.

Declaration of competing interest

The authors declare that they have no known competing financial interests or personal relationships that could have appeared to influence the work reported in this paper.

Acknowledgments

This study was partly financed by the Coordenação de Aperfeiçoamento de Pessoal de Nivel Superior - Brasil (CAPES) - Finance Code 001. The authors gratefully acknowledge the support from Brazilian National Council for Scientific and

Technological Development (CNPq) Grant 309384/2019-2 and 308056/2022-1, Carlos Chagas Filho Foundation for Supporting research in the State of Rio de Janeiro (FAPERJ) Grants E-26/202.928/2019 and E-26/201.391/2021.

REFERENCES

[1] aliakbar Hassanpouryouzband, Joonaki E, Edlmann K, Heinemann N, Yang J. Thermodynamic and transport properties of hydrogen containing streams. Sci Data 2020;7:222. https://doi.org/10.1038/s41597-020-0568-6.

[2] Lankof L, Urbańczyk K, Tarkowski R. Assessment of the potential for underground hydrogen storage in salt domes. Renew Sustain Energy Rev 2022;160. https://doi.org/10.1016/J.RSER.2022.112309.

[3] Zivar D, Kumar S, Foroozesh J. Underground hydrogen storage: a comprehensive review. Int J Hydrogen Energy 2021;46:23436–62. https://doi.org/10.1016/J.IJHYDENE.2020.08.138.

[4] Lemieux A, Sharp K, Shkarupin A. Preliminary assessment of underground hydrogen storage sites in Ontario, Canada. Int J Hydrogen Energy 2019;44:15193–204. https://doi.org/10.1016/J.IJHYDENE.2019.04.113.

[5] Liu W, Zhang Z, Chen J, Jiang D, Wu F, Fan J, et al. Feasibility evaluation of large-scale underground hydrogen storage in bedded salt rocks of China: a case study in Jiangsu province. Energy 2020;198. https://doi.org/10.1016/J.ENERGY.2020.117348.

[6] Grgic D, Al Sahyouni F, Golfier F, Moumni M, Schoumacker L. Grgic * D. Evolution of gas permeability of rock salt under different loading conditions and implications on the underground hydrogen storage in. Salt Caverns 2022;55:691–714. https://doi.org/10.1007/s00603-021-02681-y.

[7] Donadio V. Salt rock deformation and evolution: damage development and healing in rock salt. 2018.

[8] Schulze O, Popp T, Kern H. Development of damage and permeability in deforming rock salt. Eng Geol 2001;61:163–80. https://doi.org/10.1016/S0013-7952(01)00051-5.

[9] Popp T, Kern H, Schulze O. Evolution of dilatancy and permeability in rock salt during hydrostatic compaction and triaxial deformation. J Geophys Res Solid Earth 2001;106:4061–78. https://doi.org/10.1029/2000JB900381.

[10] Fuenkajorn K, Phueakphum D. Laboratory assessment of healing of fractures in rock salt. Bull Eng Geol Environ 2011;70:665–72. https://doi.org/10.1007/s10064-011-0370-y.

[11] Chen J, Ren S, Yang C, Jiang D, Li L. Self-healing characteristics of damaged rock salt under different healing conditions. Materials 2013;6:3438–50. https://doi.org/10.3390/ma6083438.

[12] Thoms RL, Gehle RM. A brief history of salt cavern use. 8th World Salt Symp. l, 2. Elsevier; 2000. p. 207–14.

[13] Bérest P. Heat transfer in salt caverns. Int J Rock Mech Min Sci 2019;120:82–95. https://doi.org/10.1016/J.IJRMMS.2019.06.009.

[14] Böttcher N, Görke U-J, Kolditz O, Nagel T. Thermo-mechanical investigation of salt caverns for short-term hydrogen storage. Environ Earth Sci 2017;76:98. https://doi.org/10.1007/s12665-017-6414-2.

[15] Caglayan DG, Weber N, Heinrichs HU, Linßen J, Robinius M, Kukla PA, et al. Technical potential of salt caverns for hydrogen storage in Europe. Int J Hydrogen Energy 2020;45:6793–805. https://doi.org/10.1016/J.IJHYDENE.2019.12.161.

[16] AbuAisha M, Rouabhi A, Billiotte J, Hadj–Hassen F. Non–isothermal two–phase hydrogen transport in rock salt during cycling in underground caverns. Int J Hydrogen Energy 2021;46:6632–47. https://doi.org/10.1016/j.ijhydene.2020.11.152.

[17] Khaledi K, Mahmoudi E, Datcheva M, Schanz T. Stability and serviceability of underground energy storage caverns in rock salt subjected to mechanical cyclic loading. 2016. https://doi.org/10.1016/j.ijrmms.2016.04.010.

[18] Maia da Costa A, V. M da Costa P, D. Udebhulu O, Cabral Azevedo R, F. F. Ebecken N, C. O. Miranda A, et al. Potential of storing gas with high CO 2 content in salt caverns built in ultra-deep water in Brazil. Greenh Gases Sci Technol 2019;9:79–94. https://doi.org/10.1002/GHG.1834.

[19] da Costa AM, Amaral CS, Poiate E, Pereira AMB, Martha LF, Gattass M, et al. Underground storage of natural gas and CO2 in salt caverns in deep and ultra-deep water offshore Brazil. 12th ISRM Congr 2011:ISRM-12 Congress-2011-300.

[20] Costa PVM, Costa AM, Poiate Jr E, Amaral CS, Pereira AMB. Computer modeling applied in the design of underground salt caverns opened by solution mining for gas storage. 49th U.S. Rock Mechanics/Geomechanics Symposium, San Francisco 2015. ARMA-2015-393.

[21] Firme PALP, Roehl D, Romanel C. Salt caverns history and geomechanics towards future natural gas strategic storage in Brazil. J Nat Gas Sci Eng 2019;72. https://doi.org/10.1016/J.JNGSE.2019.103006.

[22] Xia C, Zhou Y, Zhou S, Zhang P, Wang F. A simplified and unified analytical solution for temperature and pressure variations in compressed air energy storage caverns. Renew Energy 2015;74:718–26. https://doi.org/10.1016/J.RENENE.2014.08.058.

[23] Wang TT, Ma HL, Shi XL, Yang CH, Zhang N, Li JL, et al. Salt cavern gas storage in an ultra-deep formation in Hubei, China. Int J Rock Mech Min Sci 2018;102:57–70. https://doi.org/10.1016/J.IJRMMS.2017.12.001.

[24] Peach CJ. Influence of deformation on the fluid transport properties of salt rocks. Faculteit Aardwetenschappen der Rijksuniversiteit te Utrecht; 1991.

[25] Petersen K, Lerche I. Temperature dependence of thermal anomalies near evolving salt structures: importance for reducing exploration risk. Geol Soc London, Spec Publ 1996;100:275–90. https://doi.org/10.1144/GSL.SP.1996.100.01.18.

[26] Fairhurst C, St John CM, Midea NF, Eston SM, Fernandes AC, Bongiovanni LA. Rock Mechanics studies of proposed underground mining of potash in Sergipe, Brazil. 4th ISRM Congr 1979:131–8. https://doi.org/10.1016/0148-9062(80)91491-6.

[27] Poiate EJ. Rock mechanics and computational mechanics for the design of oil wells in salt zones. Pontifícia Universidade Católica do Rio De Janeiro; 2012.

[28] Munson DE, Fossum AF, Senseny PE. Advances in resolution of discrepancies between predicted and measured in situ WIPP (Waste Isolation Pilot Plant) room closures. 1989. https://doi.org/10.2172/5784434. Albuquerque, NM, and Livermore, CA (United States).

[29] Munson DE, Dawson PR. A workhardening/recovery model of transient creep of salt during stress loading and unloading. 1982.

[30] Mackay F, Inoue N, Fontoura SA. Geomechanical effects of a 3D vertical salt well drilling by FEA. Am Rock Mech Assoc 2008.

[31] Labaune P, Rouabhi A, Tijani M, Blanco-Martín L, You T. Dilatancy criteria for salt cavern design: a comparison between stress- and strain-based. Approaches 2018;51:599–611. https://doi.org/10.1007/s00603-017-1338-4.

Please cite this article as: Dias W et al., Cavern integrity for underground hydrogen storage in the Brazilian pre-salt fields, International Journal of Hydrogen Energy, https://doi.org/10.1016/j.ijhydene.2023.03.292

[32] Spiers CJ, Peach CJ, Brzesowsky RH, Schutjens P, Liezenberg JL, Zwart HJ. Long-term rheological and transport properties of dry and wet salt rocks. 1988.
[33] Hunsche UE. Failure behaviour of rock salt around underground cavities. Proc. 7th Symp. Salt 1993;1:59–65.
[34] Van Sambeek LL, Ratigan JL, Hansen FD. Dilatancy of rock salt in laboratory tests. Int J rock Mech Min Sci & Geomech Abstr 1993;30:735–8.
[35] Hou Z. Mechanical and hydraulic behavior of rock salt in the excavation disturbed zone around underground facilities. Int J Rock Mech Min Sci 2003;40:725–38. https://doi.org/10.1016/S1365-1609(03)00064-9.
[36] DeVries KL, Mellegard KD, Callahan GD, Goodman WM. Cavern roof stability for natural gas storage in bedded salt. 2005.
[37] Costa AM, Poiate Jr E, Falcao J. Well design for drilling through thick evaporite layers in santos basin—Brazil. In: Proc. IADC/SPE Drill. Conf. Society of Petroleum Engineers; 2006. p. 16. https://doi.org/10.2523/99161-MS. SPE 99161.
[38] Costa AM, Poiate E, Amaral CS, Pereira A, Martha LF, Gattass M, et al. Geomechanics applied to the well design through salt layers in Brazil: a history of success. Springer Ser. Geomech. Geoengin.; 2011. p. 165–8. https://doi.org/10.1007/978-3-642-19630-0_42.
[39] Costa AM, Poiate JE, Falcão JL, Coelho LFM. Triaxial creep tests in salt applied in drilling through thick salt layers in campos basin-Brazil. In: SPE/IADC Drill. Conf. Society of Petroleum Engineers; 2005. https://doi.org/10.2118/92629-MS.
[40] Firme PALP, Roehl DM, Romanel C, Poiate Jr E, Costa AM. Creep constitutive modeling applied to the stability of pre-salt wellbores through salt layers. Am Rock Mech Assoc 2014:10.
[41] Brouard B, Bérest P, De Greef V, Béraud JF, Lheur C, Hertz E. Creep closure rate of a shallow salt cavern at Gellenoncourt, France. Int J Rock Mech Min Sci 2013;62:42–50. https://doi.org/10.1016/J.IJRMMS.2012.12.030.
[42] Firme PALP, Roehl D, Romanel C. An assessment of the creep behaviour of Brazilian salt rocks using the multi-mechanism deformation model. Acta Geotech 2016;11:1445–63. https://doi.org/10.1007/s11440-016-0451-y.
[43] Zhu C, Shen X, Arson C, Pouya A. Numerical study of thermo-mechanical effects on the viscous damage behavior of rock salt caverns. 2017.
[44] Teixeira Mendes CA, Gattass M, Roehl D. The GeMA framework – an innovative framework for the development of multiphysics and multiscale simulations. In: Proc. VII Eur. Congr. Comput. Methods Appl. Sci. Eng. (ECCOMAS Congr. 2016). Athens: Institute of Structural Analysis and Antiseismic Research School of Civil Engineering National Technical University of Athens (NTUA) Greece; 2016. p. 7886–94. https://doi.org/10.7712/100016.2383.6771.
[45] Chan KS, Bodner SR, Munson DE. Permeability of WIPP salt during damage evolution and healing. 2001. https://doi.org/10.1106/H3UV-1URA-AFUY-FX49.
[46] Alkan H. Percolation model for dilatancy-induced permeability of the excavation damaged zone in rock salt. Int J Rock Mech Min Sci 2009;46:716–24. https://doi.org/10.1016/J.IJRMMS.2008.08.002.
[47] Khaledi K, Mahmoudi E, Datcheva M, Schanz T. Stability and serviceability of underground energy storage caverns in rock salt subjected to mechanical cyclic loading. Int J Rock Mech Min Sci 2016;86:115–31. https://doi.org/10.1016/J.IJRMMS.2016.04.010.

Please cite this article as: Dias W et al., Cavern integrity for underground hydrogen storage in the Brazilian pre-salt fields, International Journal of Hydrogen Energy, https://doi.org/10.1016/j.ijhydene.2023.03.292